Letter

Two-dimensional electronic conductivity in insulating ferroelectrics: Peculiar properties of domain walls

Leonard M. Verhoff [1,2,*] Mike N. Pionteck [1,3] Michael Rüsing [4] Holger Fritze [5,6] Lukas M. Eng [7,8] and Simone Sanna [1,3]

[1]*Institut für Theoretische Physik, Justus-Liebig-Universität Gießen, 35392 Gießen, Germany*
[2]*Institute for Solid State Physics, Vienna University of Technology, 1040 Vienna, Austria*
[3]*Center for Materials Research (ZfM/LaMa), Justus-Liebig-Universität Gießen, 35392 Giessen, Germany*
[4]*Department of Physics, Integrated Quantum Optics, Institute for Photonic Quantum Systems (PhoQS), Paderborn University, 33098 Paderborn, Germany*
[5]*Institute of Energy Research and Physical Technologies, Clausthal University of Technology, 38640 Goslar, Germany*
[6]*Research Center Energy Storage Technologies, Clausthal University of Technology, 38640 Goslar, Germany*
[7]*Institute of Applied Physics, Technical University Dresden, 01062 Dresden, Germany*
[8]*Dresden-Würzburg Cluster of Excellence–EXC 2147, Technical University Dresden, 01062 Dresden, Germany*

(Received 16 April 2024; accepted 6 September 2024; published 15 October 2024)

Ferroelectrics such as $LiNbO_3$ (LN) are wide-band-gap insulators that may show a high local electric conductivity at the domain walls (DWs). The latter are interfaces separating regions of noncollinear polarization, which can be manipulated to build integrated nanoelectronic elements. In the present work, we model different DW types in LN from first principles. Our models reveal the DW morphology and shed light on their electronic properties: A strong band bending is predicted for charged DWs, leading to local metallicity. Defect trapping at the DW may further enhance the electric conductivity.

DOI: 10.1103/PhysRevResearch.6.L042015

The electric conductivity of ferroelectric domain walls (DWs) in large-band-gap semiconductors can be orders of magnitude larger than in the surrounding bulk material [1–5]. DWs can be manipulated, e.g., precisely positioned and controlled by the use of electrical fields [6]. Consequently, DWs can be exploited to incorporate quasi-two-dimensional (2D) rewritable conduction paths across pure (undoped) and otherwise insulating materials. As DWs, and therefore their electrical conductivity, are usually confined to a few unit cells [7], nanoscopic circuits [8] become realizable. Although DWs already find applications in nanoelectronics [5,9,10], our knowledge of their atomic structure is limited to few materials [11–14] and little is known about the mechanisms leading to the large conductivity [15–18]. Three major mechanisms have been proposed to explain the high conductivity of DWs [10]: A DW could either (i) intrinsically reshape the band structure, (ii) host a high density of intrinsic defects, or (iii) locally bend the conduction and valence bands.

Although these suggestions have been partially confirmed, e.g., for the multiferroic $YMnO_3$ [19], for most ferroelectrics a reliable theoretical basis for DW conductivity that goes beyond a phenomenological explanation is still missing. This also holds for lithium niobate [$LiNbO_3$ (LN)]—the most prominent electro-optical material—which we investigate here as a prototypical proper ferroelectric. LN is indeed an uniaxial ferroelectric, i.e., the spontaneous polarization is only oriented along the crystallographic z-axis, unlike other typical perovskite materials such as $BaTiO_3$ or $PbTiO_3$, in which different polarization axes exist. This peculiarity reduces the number of possible DW orientations.

In this work, we model DWs in LN in the framework of density functional theory (DFT). The models give insight into the ionic and electronic structure around DWs. For the investigation, we chose DWs that are orthogonal to the three main Cartesian axes [x- and y-axis defined as in Fig. 1(b)]. DWs parallel to the xz- and yz-plane (X- and Y-walls, respectively) are nominally uncharged. At DWs parallel to the xy-plane, polarization meets *head-to-head* (H2H) or *tail-to-tail* (T2T), leading to highly charged interfaces. Any real-world DW can be described as a combination of these three wall types [7].

We find the so-called H2H and T2T DWs to be morphologically different and in both cases charged. The spatially resolved density of states (DOS) provides an explanation for the mechanism leading to the electric conductivity. Moreover, favorable conditions for defect formations at DWs are found. The results can be qualitatively transferred to isomorph ferroelectrics such as $LiTaO_3$; the applied methodology can be extended to more complex ferroelectrics, such as $BiFeO_3$, $BaTiO_3$, or $ErMnO_3$.

In the high-symmetry, paraelectric phase of LN (space group $R\bar{3}c$ above 1165 °C [20]), the Nb ions lie right in the

*Contact author: leonard.verhoff@tuwien.ac.at

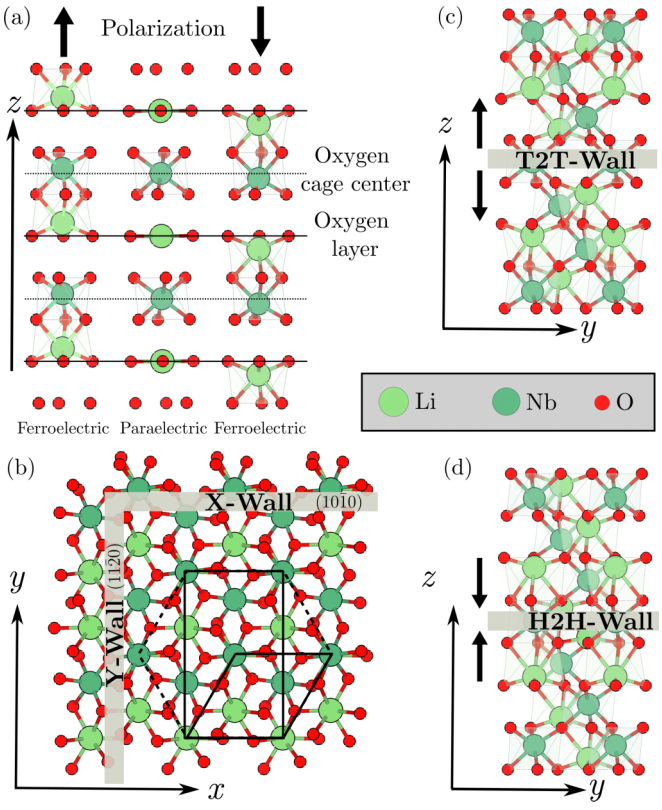

FIG. 1. (a) The paraelectric (center) and the equivalent ferroelectric configurations of LN, with the spontaneous polarization being aligned parallel (left) and antiparallel (right) to the z-direction. (b) Top view of LN, featuring the orthorhombic and hexagonal unit cells as black lines, and X- and Y-walls as gray regions. (c) and (d) Ionic structure around H2H and T2T walls, respectively, projected onto the yz-plane.

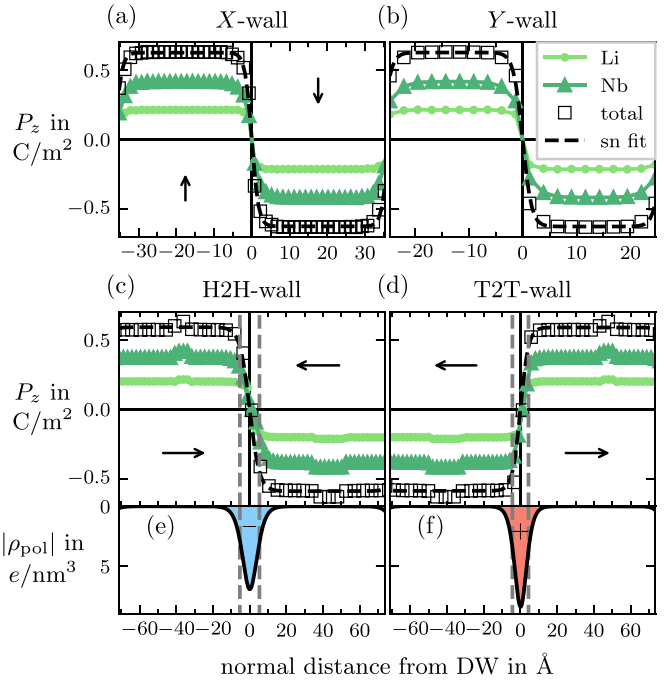

FIG. 2. (a)–(d) Spontaneous polarization as a function of the distance to the DW around X-, Y-, H2H-, and T2T-walls. Total polarization is the sum of Li and Nb contribution, fitted with a Jacobi elliptic function (sn). Arrows indicate the direction of spontaneous polarization. (e) and (f) Screening charges around H2H and T2T DW: blue indicates an accumulation, red a depletion of negative charges. Dashed lines visualize the half-widths x_L.

center of an O octahedron, while the Li ions are located within an O *layer* [Fig. 1(a)]. This inversion-symmetric configuration provides the reference paraelectric phase, characterized by the spontaneous polarization $P_z = 0$.

Below the Curie temperature T_C, inversion symmetry is spontaneously broken, and a ferroelectric configuration emerges by a second-order phase transition. The Nb sublattice collectively moves in either the positive (upwards) or negative (downwards) z-direction, while the Li sublattice arranges correspondingly either above or below the oxygen layer. Although the crystal's threefold rotational symmetry is preserved, the phase transition displaces the center of positive charges relative to the center of negative charges, and hence causes a net dipole moment. In turn, this defines a scalar order parameter—the spontaneous polarization P_z. The two resulting (energetically equivalent) low-temperature phases belonging to the $R3c$ space group are illustrated to the left- and right-hand side of Fig. 1(a), respectively. With lowering temperature, the order parameter grows continuously and reaches its maximum value P_s at $T = 0$ [21].

The existence of two ferroelectric configurations implies the existence of regions of opposite polarization, coexisting in real crystals and separated by a DW. The DW can be seen as an extended defect locally perturbing the otherwise perfect lattice. The scalar order parameter P_z thus becomes an order parameter field which, approximately, only depends on the distance from the DW.

The X- and Y-DWs modeled in this work are sketched in Fig. 1(b). Due to the peculiar atomic layer stacking along the y-axis, two nonequivalent X-DWs exist [22,23]. Our calculations [computational details can be found in the Supplemental Material (SM) [24]] reveal that the most stable position of X- and Y-DWs within the crystal is, in all cases, right between two cationic planes. The spontaneous polarization vectors on either side of the DW align parallel to the domain wall, but are rotated by 180° relative to each other.

The calculated polarization profile around the DWs is monotonic and well-defined, although it changes its sign over a small width, as shown in Figs. 2(a) and 2(b). Scrymgeour *et al.* [25] used the Ginzburg-Landau-Devonshire theory (GLD) to show that the profile of polarization follows a (continuous) Jacobi elliptic function $\mathrm{sn}(x_n/x_L, k)$, where x_n is the distance from the wall, x_L quantifies the DW half-width, and k is the modulus, determined by the distance between two walls. The polarization profile becomes a hyperbolic tangent function in the limit of two semi-infinite domains. Our atomistic models confirm the derived analytic profile, and they are in agreement with previous simulations based on empirical potentials [22,26]. As previously pointed out [21], the Nb sublattice yields the largest contribution to the polarization. The ionic lattice distortions appear mostly in the vicinity of the DWs: 99% of bulk polarization is reached

at a distance of 5.3 Å (X-walls; $x_L = 1.78$ Å) and 4.7 Å (Y-walls; $x_L = 1.67$ Å), hinting at the strongly pronounced two-dimensionality of DWs.

According to GLD, a nonzero normal polarization establishes close to an X-wall, due to the rotation of the polarization out of the DW plane (Néel type DW), which is also supported by second-harmonic generation polarimetry studies [27,28]. Our calculations indeed reveal a polarization component P_n perpendicular to the X-DW as low as 7.5 $\mu C/cm^2$. Gauss's law states that the normal polarization P_n around X-walls causes a bound charge density, proportional to the slope of P_n. Consequently, a small amount of free charge carriers (from defects and impurities) accumulates around the X-walls to screen the bound surface charge. Due to the small magnitude of P_n, this effect can hardly explain the experimentally observed DW's conductivity.

For H2H and T2T walls (see Fig. 1), the described mechanism becomes relevant: Free negative charges accumulate around H2H DWs, leaving a depletion of negative charges around T2T DWs. The absolute change of $2P_s$ from $+P_s$ to $-P_s$ within a few Å results in a large amount of charge carriers needed to screen the bound interface charge. Therefore, H2H and T2T DWs are often referred to as *charged* DWs. Our structural relaxation reveals both charged DWs to be much wider than X- or Y-DWs—the spontaneous polarization in Figs. 2(c) and 2(d) shows a 99% saturation at 14.2 Å (H2H; $x_L = 5.33$ Å) and 11.7 Å (T2T; $x_L = 4.39$ Å) away from the respective DW. Consequently, the slopes of the calculated polarization profiles [Figs. 2(e) and 2(f)] suggest that the majority of free screening charges ρ_f accumulate within a region of about 1–3 nm around the DW. This is lower than the estimation of 10–100-nm-wide DWs in $BaTiO_3$ [29]. Although similar to each other, the polarization profiles at H2H and T2T DWs are not identical. A prerequisite for the existence of charged DWs is that their bound charge is almost completely screened by free charges, e.g., by the formation of a 2D electron (or hole) gas [30]. Assuming a (nonlinear) screening with a degenerate electron gas (as expected for perovskite materials far from the transition temperature), analytical expressions for the widths of charged DWs can be derived within the GLD theory [30]. Application to LN yields charged DW widths of about 4.5–5.5 Å, in agreement with the atomistic calculations. Whether the formation of 2DEG is a reasonable assumption is discussed in the following sections. A table with the calculated half-widths and 99% widths for all DW types can be found in the SM [24].

To further explore the differences between H2H and T2T DWs, and to assess whether they can explain the measured conductivity, we investigate the electronic charge at the Fermi energy. The charge density of a relaxed cell, integrated within a range of 0.1 eV from the Fermi level and averaged in the xy-plane, is shown in Fig. 3 (gray line). The curves (see red lines for the fast Fourier transformation-filtered curve) qualitatively confirm the electrostatic consideration based on Gauss's law (black lines) on a quantum-mechanical level, while the fits with Jacobi elliptic functions yield similar DW half-widths x_L. Again, due to the different nature of the DWs, the charge profiles are different and confirm that H2H DWs are somewhat broader than T2T DWs. The lower panel in Fig. 3 shows the spatial distribution of the charge density at

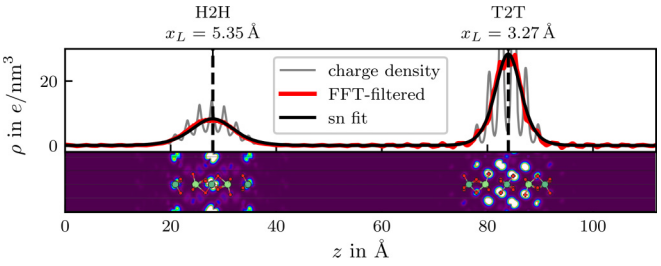

FIG. 3. Charge density at the Fermi energy along the z-direction calculated for a supercell containing charged DWs (gray line). In the red curve, high-frequency components are filtered out. Black is a fit of the charge density curve according to GLD. The lower panel shows the spatial distribution of the charge density in an xz-plane.

the Fermi level in the xz-plane, further remarking the differences between T2T and H2H DWs. The accumulation of charge carriers at the Fermi energy is an indicator of the DW conductivity. Further insight into the origin of free charges is provided by the electronic structure: The total electronic DOS is depicted in Figs. 4(a)–4(d) for bulk LN and supercells containing two X-, Y-, and charged DWs, respectively. In bulk LN, DFT calculations predict a fundamental band gap of 3.4 eV, O p-orbitals providing the valence-band states, and Nb d-orbitals providing most of the conduction-band states. We calculate a reduction of the band gap to 3.0 eV for both X- and Y-DWs, due to the energetic lowering of conduction-band states, which is also computationally found for DWs in $BiFeO_3$ [31].

For the supercells containing charged DWs [Fig. 4(d)], the band-gap reduction is extreme and leads to a closing of the band gap. The DOS in Fig. 4(d) consequently suggests a semimetallic behavior and an enhanced electrical conductivity.

The band-gap dependence on the DW orientation suggests the possibility to experimentally characterize the type of DW with optoelectronic experiments, such as photoemission or impedance spectroscopy, which for (conductive) DWs is still largely missing.

The calculation of atomic projected DOS allows the estimation of a spatially resolved, local DOS (LDOS) [Figs. 4(e)–4(g)]. The band edges of bulk LN [Fig. 4(e), central panel] show no dependency on the position within the supercell, as expected for a homogeneous crystal. However, in the supercells containing X- and Y-walls, we observe electronic states close to the conduction band that cause the overall band-gap reduction to 3.0 eV, observed in Figs. 4(b) and 4(c).

The LDOS calculated for the supercell containing the charged DWs [Figs. 4(e) and 4(f), right panel] shows a massive bending of the valence and conduction band in the vicinity of a charged DW. Both the valence- and conduction-band states are shifted towards smaller energies around H2H walls, and they are *nearly* symmetrically shifted towards larger energies around T2T walls. The magnitude of bending is large enough such that the conduction-band minimum at H2H walls and the valence-band maximum at T2T walls overlap by a narrow energy interval of about 0.5 eV [Fig. 4(g)]. A similar band bending was also obtained in phase-field

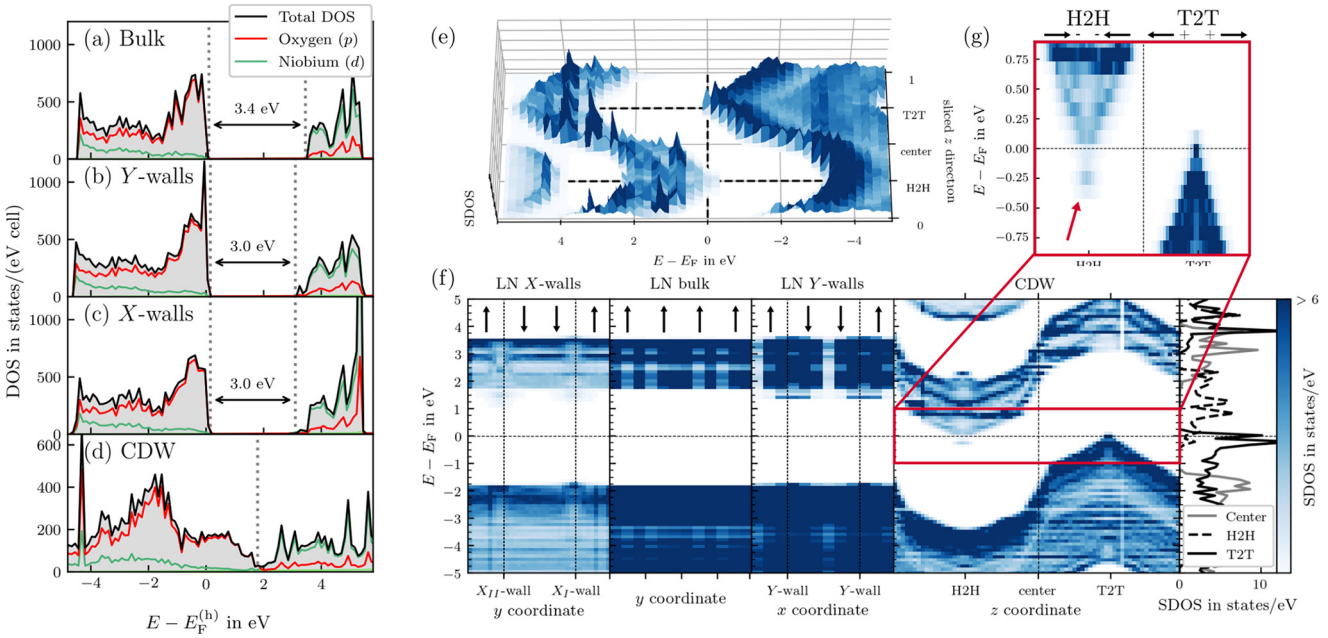

FIG. 4. DFT-calculated total (a)–(d) and local (e)–(g) DOS of LN for different wall types. From left to right in the lower row: LDOS for X-walls, bulk material, Y-walls, and charged DWs (CDW). Panel (g) is a magnification of the inset of (f) showing the overlap of VBM and CBM.

simulations of $BaTiO_3$ [32]. The calculations of DOS presented above are performed with semilocal xc-functionals [33], which are known to underestimate the band gap for most systems. To test the validity of our approach, we also perform calculations with the more sophisticated and computationally demanding hybrid-DFT in a HSE06 fashion [34,35] (see SM [24] for details). The semimetallic behavior of supercells modeling charged DWs is confirmed by hybrid-DFT and is therefore not a computational artifact. In addition, the magnitude of the band overlap is converged with respect to the DW distance (or supercell size). However, a reliable numerical value of the overlap would require more refined band-structure methods [36].

The magnification in Fig. 4(g) reveals that electronic states—separated by about 0.25 eV from the conduction-band tip—emerge at the H2H wall. These states, absent in the bulk material, are provided by the Nb ions [Fig. 1(d); for more details, see the SM [24]]. They might be related to the activation energies of about 0.10–0.25 eV measured in LN by Zahn *et al.* [1,37]. These electronic states are not present at the T2T DW, and they introduce an asymmetry in the LDOS. This asymmetry could also explain why the measured conductivity at H2H walls is higher than at T2T walls [3,38]. Unfortunately, a quantitative comparison with experimental results is not possible at this stage, as perfectly straight H2H or T2T DWs as modeled in the present work are difficult to realize in LN [39,40].

The vanishing band gap [Fig. 4(d)], in combination with the spatial confinement of charges at the Fermi level (Fig. 3), suggests the formation of a (quasi-)two-dimensional electron gas (2DEG) at charged DWs, as observed in $BaTiO_3$ [29,38] and proposed for $LiNbO_3$ [41]. Whether the 2DEG can explain the conductivity in real *inclined* DWs remains to be investigated in upcoming studies. Instead, we discuss a further effect that might contribute to enhance the DW conductivity, namely the defect accumulation at the DW. In particular, the presence of small polarons, which are responsible for the electronic contribution to the LN conductivity via electron hopping, might provide a further conduction mechanism [42–46]. As the simulation of defects at charged DWs requires huge supercells, we adopt here a simplified approach. Previous studies based on XRD spectroscopy have revealed that DWs in LN can be viewed, in first approximation, as compressed bulk [47,48]. Thus, we consider small bound Nb_{Li} polarons and bipolarons within a compressed bulk to model their occurrence at DWs. Our models (see the SM [24] for further details concerning the considered strain and its realization) demonstrate that the formation energy of polarons and bipolarons rapidly decreases with the applied strain. Thus, higher defect concentrations are expected at the DW, which can further contribute to the electric conductivity.

Summarizing, we modeled X-, Y-, and charged DWs in LN. The DFT-calculated DOS provides a mechanism for the origin of electric conductivity of the charged DWs in the large band-gap semiconductor. The large band bending, the appearing shallow states, and defect accumulation contribute to the conductivity. The relative magnitude of these effects shall be assessed in further investigations. In reality, it is hard to fabricate DWs perfectly orthogonal to the z-axis—which matches our observation of the DFT-calculated DW formation energy for charged DWs being about one magnitude larger than for X- and Y-DWs. The highly conductive DWs studied experimentally, therefore, often show a small but nonzero inclination angle with respect to the z-axis [3,49]. Even the plain X- and Y-DWs are not perfectly straight: On a microscopic scale, they rather show a meandering interface [7]. This suggests that an inclined DW would be realized by a combination of the high-symmetry walls studied in this work,

which thus represents a further step toward understanding and manipulating charged DWs.

The modeling of DWs in LN paves the way for many more applications: $LiTaO_3$ (LT), for instance, is isostructural to LN. Interfaces of LN and LT, which can be experimentally realized (through, e.g., bonding) can be simulated. These interfaces, as well as the employment of LN-LT solid solution, or the application to thin films [50,51], may help to precisely tune the polarization and the electronic properties around DWs. Moreover, our computational approach combining phenomenological and atomistic models can be directly extended to study more complex (multi)ferroics such as $BiFeO_3$ or $ErMnO_3$ featuring more than one polarization axis, their thin films [52], or further nonperovskite ferroelectrics.

We gratefully acknowledge financial support by the Deutsche Forschungsgemeinschaft (Grant No. 426703838). Calculations for this research were conducted on the Lichtenberg high-performance computer of the TU Darmstadt, at the Höchstleistungrechenzentrum Stuttgart (HLRS), and at the HPC Core Facility of the Justus-Liebig-Universität Gießen.

[1] M. Zahn, E. Beyreuther, I. Kiseleva, A. S. Lotfy, C. J. McCluskey, J. R. Maguire, A. Suna, M. Rüsing, J. M. Gregg, and L. M. Eng, Equivalent-circuit model that quantitatively describes domain-wall conductivity in ferroelectric $LiNbO_3$, Phys. Rev. Appl. **21**, 024007 (2024).

[2] L. Liu, K. Xu, Q. Li, J. Daniels, H. Zhou, J. Li, J. Zhu, J. Seidel, and J.-F. Li, Giant domain wall conductivity in self-assembled $BiFeO_3$ nanocrystals, Adv. Funct. Mater. **31**, 2005876 (2021).

[3] E. Singh, H. Beccard, Z. H. Amber, J. Ratzenberger, C. W. Hicks, M. Rüsing, and L. M. Eng, Tuning domain wall conductivity in bulk lithium niobate by uniaxial stress, Phys. Rev. B **106**, 144103 (2022).

[4] J. R. Whyte, R. G. P. McQuaid, P. Sharma, C. Canalias, J. F. Scott, A. Gruverman, and J. M. Gregg, Domain walls: Ferroelectric domain wall injection, Adv. Mater. **26**, 348 (2014).

[5] G. Catalan, J. Seidel, R. Ramesh, and J. F. Scott, Domain wall nanoelectronics, Rev. Mod. Phys. **84**, 119 (2012).

[6] C. Godau, T. Kämpfe, A. Thiessen, L. M. Eng, and A. Haußmann, Enhancing the domain wall conductivity in lithium niobate single crystals, ACS Nano **11**, 4816 (2017).

[7] J. Gonnissen, D. Batuk, G. F. Nataf, L. Jones, A. M. Abakumov, S. Van Aert, D. Schryvers, and E. K. H. Salje, Direct observation of ferroelectric domain walls in $LiNbO_3$: Wall-meanders, kinks, and local electric charges, Adv. Funct. Mater. **26**, 7599 (2016).

[8] L. Chua, Memristor-the missing circuit element, IEEE Trans. Circ. Theor. **18**, 507 (1971).

[9] J. Wang, J. Ma, H. Huang, J. Ma, H. M. Jafri, Y. Fan, H. Yang, Y. Wang, M. Chen, D. Liu, J. Zhang, Y.-H. Lin, L.-Q. Chen, D. Yi, and C.-W. Nan, Ferroelectric domain-wall logic units, Nat. Commun. **13**, 3255 (2022).

[10] G. F. Nataf, M. Guennou, J. M. Gregg, D. Meier, J. Hlinka, E. K. H. Salje, and J. Kreisel, Domain-wall engineering and topological defects in ferroelectric and ferroelastic materials, Nat. Rev. Phys. **2**, 634 (2020).

[11] S. Liu and R. E. Cohen, Stable charged antiparallel domain walls in hyperferroelectrics, J. Phys.: Condens. Matter **29**, 244003 (2017).

[12] D. R. Småbråten, Q. N. Meier, S. H. Skjærvø, K. Inzani, D. Meier, and S. M. Selbach, Charged domain walls in improper ferroelectric hexagonal manganites and gallates, Phys. Rev. Mater. **2**, 114405 (2018).

[13] U. Petralanda, M. Kruse, H. Simons, and T. Olsen, Oxygen vacancies nucleate charged domain walls in ferroelectrics, Phys. Rev. Lett. **127**, 117601 (2021).

[14] S. Liu, I. Grinberg, and A. M. Rappe, Intrinsic ferroelectric switching from first principles, Nature (London) **534**, 360 (2016).

[15] P. S. Bednyakov, B. I. Sturman, T. Sluka, A. K. Tagantsev, and P. V. Yudin, Physics and applications of charged domain walls, npj Comput. Mater. **4**, 65 (2018).

[16] P. Sharma, A. N. Morozovska, E. A. Eliseev, Q. Zhang, D. Sando, N. Valanoor, and J. Seidel, Specific conductivity of a ferroelectric domain wall, ACS Appl. Electron. Mater. **4**, 2739 (2022).

[17] D. Lee, R. K. Behera, P. Wu, H. Xu, Y. L. Li, S. B. Sinnott, S. R. Phillpot, L. Q. Chen, and V. Gopalan, Mixed Bloch-Néel-Ising character of 180° ferroelectric domain walls, Phys. Rev. B **80**, 060102(R) (2009).

[18] J. Guyonnet, E. Agoritsas, S. Bustingorry, T. Giamarchi, and P. Paruch, Multiscaling analysis of ferroelectric domain wall roughness, Phys. Rev. Lett. **109**, 147601 (2012).

[19] D. Meier, J. Seidel, A. Cano, K. Delaney, Y. Kumagai, M. Mostovoy, N. A. Spaldin, R. Ramesh, and M. Fiebig, Anisotropic conductance at improper ferroelectric domain walls, Nat. Mater. **11**, 284 (2012).

[20] R. S. Weis and T. K. Gaylord, Lithium niobate: Summary of physical properties and crystal structure, Appl. Phys. A. **37**, 191 (1985).

[21] F. Bernhardt, L. M. Verhoff, N. A. Schäfer, A. Kapp, C. Fink, W. A. Nachwati, U. Bashir, D. Klimm, F. E. Azzouzi, U. Yakhnevych, Y. Suhak, H. Schmidt, K.-D. Becker, S. Ganschow, H. Fritze, and S. Sanna, Ferroelectric to paraelectric structural transition in $LiTaO_3$ and $LiNbO_3$, Phys. Rev. Mater. **8**, 054406 (2024).

[22] D. Lee, H. Xu, V. Dierolf, V. Gopalan, and S. R. Phillpot, Structure and energetics of ferroelectric domain walls in $LiNbO_3$ from atomic-level simulations, Phys. Rev. B **82**, 014104 (2010).

[23] S. Sanna and W. G. Schmidt, $LiNbO_3$ surfaces from a microscopic perspective, J. Phys.: Condens. Matter **29**, 413001 (2017).

[24] See Supplemental Material at http://link.aps.org/supplemental/10.1103/PhysRevResearch.6.L042015 for computational details and convergence tests.

[25] D. A. Scrymgeour, V. Gopalan, A. Itagi, A. Saxena, and P. J. Swart, Phenomenological theory of a single domain wall in uniaxial trigonal ferroelectrics: Lithium niobate and lithium tantalate, Phys. Rev. B **71**, 184110 (2005).

[26] A. J. Klomp, R. Khachaturyan, T. Wallis, K. Albe, and A. Grünebohm, Thermal stability of nanoscale ferroelectric do-

mains by molecular dynamics modeling, Phys. Rev. Mater. **6**, 104411 (2022).

[27] S. Cherifi-Hertel, H. Bulou, R. Hertel, G. Taupier, K. D. H. Dorkenoo, C. Andreas, J. Guyonnet, I. Gaponenko, K. Gallo, and P. Paruch, Non-ising and chiral ferroelectric domain walls revealed by nonlinear optical microscopy, Nat. Commun. **8**, 15768 (2017).

[28] U. Acevedo-Salas, B. Croes, Y. Zhang, O. Cregut, K. D. Dorkenoo, B. Kirbus, E. Singh, H. Beccard, M. Rüsing, L. M. Eng, R. Hertel, E. A. Eliseev, A. N. Morozovska, and S. Cherifi-Hertel, Impact of 3d curvature on the polarization orientation in non-ising domain walls, Nano Lett. **23**, 795 (2023).

[29] T. Sluka, A. K. Tagantsev, P. Bednyakov, and N. Setter, Free-electron gas at charged domain walls in insulating $BaTiO_3$, Nat. Commun. **4**, 1808 (2013).

[30] M. Y. Gureev, A. K. Tagantsev, and N. Setter, Head-to-head and tail-to-tail 180° domain walls in an isolated ferroelectric, Phys. Rev. B **83**, 184104 (2011).

[31] A. Lubk, S. Gemming, and N. A. Spaldin, First-principles study of ferroelectric domain walls in multiferroic bismuth ferrite, Phys. Rev. B **80**, 104110 (2009).

[32] T. Sluka, A. Tagantsev, and D. Damjanovic, Enhanced electromechanical response of ferroelectrics due to charged domain walls, Nat. Commun. **3**, 748 (2012).

[33] J. P. Perdew, K. Burke, and M. Ernzerhof, Generalized gradient approximation made simple, Phys. Rev. Lett. **77**, 3865 (1996).

[34] J. Heyd, G. E. Scuseria, and M. Ernzerhof, Hybrid functionals based on a screened Coulomb potential, J. Chem. Phys. **118**, 8207 (2003).

[35] J. Heyd, G. E. Scuseria, and M. Ernzerhof, Erratum: Hybrid functionals based on a screened Coulomb potential [The Journal of Chemical Physics 118, 8207 (2003)], J. Chem. Phys. **124**, 219906(E) (2006).

[36] K. Held, Electronic structure calculations using dynamical mean field theory, Adv. Phys. **56**, 829 (2007).

[37] U. Yakhnevych, M. Kunzner, L. M. Verhoff, J. Ratzenberger, E. Beyreuther, M. Rüsing, S. Sanna, L. M. Eng, and H. Fritze, High-temperature domain wall current in Mg-doped lithium niobate single crystals up to 400°C, arXiv:2404.01214.

[38] H. Beccard, B. Kirbus, E. Beyreuther, M. Rüsing, P. Bednyakov, J. Hlinka, and L. M. Eng, Nanoscale conductive sheets in ferroelectric $BaTiO_3$: Large hall electron mobilities at head-to-head domain walls, ACS Appl. Nano Mater. **5**, 8717 (2022).

[39] H. Lu, Y. Tan, J. P. V. McConville, Z. Ahmadi, B. Wang, M. Conroy, K. Moore, U. Bangert, J. E. Shield, L.-Q. Chen, J. M. Gregg, and A. Gruverman, Electrical tunability of domain wall conductivity in $LiNbO_3$ thin films, Adv. Mater. **31**, 1902890 (2019).

[40] V. Y. Shur, E. L. Rumyantsev, E. V. Nikolaeva, and E. I. Shishkin, Formation and evolution of charged domain walls in congruent lithium niobate, Appl. Phys. Lett. **77**, 3636 (2000).

[41] H. Beccard, E. Beyreuther, B. Kirbus, S. D. Seddon, M. Rüsing, and L. M. Eng, Hall mobilities and sheet carrier densities in a single $LiNbO_3$ conductive ferroelectric domain wall, Phys. Rev. Appl. **20**, 064043 (2023).

[42] U. Yakhnevych, F. E. Azzouzi, F. Bernhardt, C. Kofahland, Y. Suhak, S. Sanna, K. D. Becker, H. Schmid, S. Ganschow, and H. Fritze, Oxygen partial pressure and temperature dependent electrical conductivity of lithium-niobate-tantalate solid solutions, Solid State Ion. **407**, 116487 (2024).

[43] D. Smyth, Defects and transport in $LiNbO_3$, Ferroelectrics **50**, 93 (1983).

[44] O. Schirmer, M. Imlau, C. Merschjahn, and B. Schike, Electron small polarons and bipolarons in $LiNbO_3$, J. Phys.: Condens. Matter **21**, 123201 (2009).

[45] C. Kofahl, L. Dörrer, B. Muscutt, S. Sanna, S. Hurskyy, U. Yakhnevych, Y. Suhak, H. Fritze, S. Ganschow, and H. Schmidt, Li self-diffusion and ion conductivity in congruent $linbo_3$ and $litao_3$ single crystals, Phys. Rev. Mater. **7**, 033403 (2023).

[46] E. Ghorbani, L. Villa, P. Erhart, A. Klein, and K. Albe, Self-consistent calculations of charge self-trapping energies: A comparative study of polaron formation and migration in $PbTiO_3$, Phys. Rev. Mater. **6**, 074410 (2022).

[47] T. Jach, S. Kim, V. Gopalan, S. Durbin, and D. Bright, Long-range strains and the effects of applied field at 180° ferroelectric domain walls in lithium niobate, Phys. Rev. B **69**, 064113 (2004).

[48] M. Rüsing, S. Neufeld, J. Brockmeier, C. Eigner, P. Mackwitz, K. Spychala, C. Silberhorn, W. G. Schmidt, G. Berth, A. Zrenner, and S. Sanna, Imaging of 180° ferroelectric domain walls in uniaxial ferroelectrics by confocal raman spectroscopy: Unraveling the contrast mechanism, Phys. Rev. Mater. **2**, 103801 (2018).

[49] T. Kämpfe, P. Reichenbach, A. Haußmann, T. Woike, E. Soergel, and L. M. Eng, Real-time three-dimensional profiling of ferroelectric domain walls, Appl. Phys. Lett. **107**, 152905 (2015).

[50] C. Weymann, S. Cherifi-Hertel, C. Lichtensteiger, I. Gaponenko, K. D. Dorkenoo, A. B. Naden, and P. Paruch, Non-ising domain walls in *c*-phase ferroelectric lead titanate thin films, Phys. Rev. B **106**, L241404 (2022).

[51] J. R. Maguire, C. J. McCluskey, K. M. Holsgrove, A. Suna, A. Kumar, R. G. P. McQuaid, and J. M. Gregg, Ferroelectric domain wall p-n junctions, Nano Lett. **23**, 10360 (2023).

[52] J. Sifuna, P. García-Fernández, G. S. Manyali, G. Amolo, and J. Junquera, First-principles study of two-dimensional electron and hole gases at the head-to-head and tail-to-tail 180° domain walls in $PbTiO_3$ ferroelectric thin films, Phys. Rev. B **101**, 174114 (2020).